Contact angle measurement for hydrogen/brine/sandstone system using captive-bubble method relevant for underground hydrogen storage

Hashemi, Leila; Glerum, Wuis ; Farajzadeh, Rouhi; Hajibeygi, Hadi

DOI
10.1016/j.advwatres.2021.103964

Publication date
2021

Document Version
Final published version

Published in
Advances in Water Resources

Advances in Water Resources 154 (2021) 103964

Contents lists available at ScienceDirect

Advances in Water Resources

journal homepage: www.elsevier.com/locate/advwatres

Contact angle measurement for hydrogen/brine/sandstone system using captive-bubble method relevant for underground hydrogen storage

Leila Hashemi, Wuis Glerum, Rouhi Farajzadeh, Hadi Hajibeygi*

Faculty of Civil Engineering and Geosciences, Delft University of Technology, P.O. Box 5048, Delft, GA 2600, The Netherlands

ARTICLE INFO

Keywords:
Underground hydrogen storage
Contact angle
Hydrogen/brine/sandstone
Wettability

ABSTRACT

Subsurface porous formations provide large capacities for underground hydrogen storage (UHS). Successful utilization of these porous reservoirs for UHS depends on accurate quantification of the hydrogen transport characteristics at continuum (macro) scale, specially in contact with other reservoir fluids. Relative-permeability and capillary-pressure curves are among the macro-scale transport characteristics which play crucial roles in quantification of the storage capacity and efficiency. For a given rock sample, these functions can be determined if pore-scale (micro-scale) surface properties, specially contact angles, are known. For hydrogen/brine/rock system, these properties are yet to a large extent unknown. In this study, we characterize the contact angles of hydrogen in contact with brine and Bentheimer and Berea sandstones at various pressure, temperature, and brine salinity using captive-bubble method. The experiments are conducted close to the in-situ conditions, which resulted in water-wet intrinsic contact angles, about 25 to 45 degrees. Moreover, no meaningful correlation was found with changing tested parameters. We monitor the bubbles over time and report the average contact angles with their minimum and maximum variations. Given rock pore structures, using the contact angles reported in this study, one can define relative-permeability and capillary-pressure functions for reservoir-scale simulations and storage optimization.

1. Introduction

Successful transition towards low-carbon energy systems depends not only on harvesting more renewable resources but also on advancements of large-scale (TWh) storage technologies. Renewable energy can be stored in TWh scales, if it is converted into green molecules such as hydrogen. The green hydrogen can then be stored in underground geological formations, e.g., in depleted hydrocarbon reservoirs and saline aquifers (Gabrielli et al., 2020; Stone et al., 2009; Rudolph, 2019).

Several research studies and a few pilot tests related to underground hydrogen storage (UHS) in porous reservoirs have been recently initiated (Tarkowski, 2019; Panfilov et al., 2012; Panfilov, 2016; Nemati et al., 2020; Ebrahimiyekta, 2017). UHS in porous formations still remains a challenge, due to lack of characterization data needed as input parameters to perform reservoir simulation and robust storage optimization. Among these input parameters, hydrogen surface properties in contact with reservoir fluids, especially brine, are crucially important (Heinemann et al., 2021).

To date, there exists only two experiments for characterizing hydrogen contact angle in subsurface systems. First, a coreflooding test was performed in which hydrogen was injected in brine-saturated Vosges sandstone rock at two different pressure (P) and temperature (T) values of (50 bar, 20 °C) and (100 bar, 45 °C) (Yekta et al., 2018). It resulted in receding contact angles of 21.56° and 34.9°, respectively, for the first and second (P,T) values (Yekta et al., 2018). More recently, another study was performed in which receding and advancing contact angles were measured using tilted plate experimental technique (Iglauer et al., 2021). That study was performed at pressure range of 0.1–25 MPa and temperature range of 296–343 K. Both pure and aged quartz samples were used with stearic acid in contact with brine (10 wt% NaCl). The study reported that the increase of pressure or temperature resulted in increasing contact angles from 0° to maximum of around 50° for pure quartz. However, when the quartz samples were aged for several months with stearic acid, intermediate wetting conditions were observed (Iglauer et al., 2021).

Despite its crucial impact in successful development of UHS technology, to date, there exists no hydrogen-specific dataset in general, nor contact angle measurements across scales, to allow for reliable site selection, development, and storage optimization (Ebigbo et al., 2013; Hagemann et al., 2016; Sainz-Garcia et al., 2017; Tarkowski, 2019; Luboń and Tarkowski, 2020; Flesch et al., 2018; Ozarslan, 2012; Panfilov et al., 2012). Specially once the contact angles are known, for a given rock

* Corresponding author.
E-mail addresses: L.Hashemi@tudelft.nl (L. Hashemi), W.H.P.Glerum@student.tudelft.nl (W. Glerum), R.Farajzadeh@tudelft.nl (R. Farajzadeh), h.hajibeygi@tudelft.nl (H. Hajibeygi).

https://doi.org/10.1016/j.advwatres.2021.103964
Received 31 March 2021; Received in revised form 19 May 2021; Accepted 20 May 2021
Available online 25 May 2021

type, one can perform pore-scale modelling to find upscaled relative-permeability and capillary-pressure curves (Hashemi et al., 2021; Klise et al., 2016; Liu et al., 2018; Berg et al., 2016). These functions will be used as input parameters for reservoir scale simulation studies (Blunt, 2017; Kunz et al., 2018; Rücker et al., 2019). Note that contact angles in cyclic storage transport is hysteretic (Morrow, 1975; Yang et al., 1999).

To resolve this knowledge gap, in this work, we perform contact angle measurements for hydrogen/brine/sandstone rock using a captive-bubble cell device. Since, there is no external viscous forces to displace fluid and gas phases, our study allows for nearly static (intrinsic) contact angle measurements for hydrogen when it comes in contact with the saturated porous reservoir rock. We first benchmark our measurements for nitrogen gas with the published literature, and then introduce hydrogen gas in the system. Table 8 and Table 9, in the appendix, provide a summary of different contact angle measurement methods in the systems of gas/brine/solid surface. The study is performed under different pressure, temperature and salinity of the brine; so to represent a fair assessment of the in situ conditions. Our findings shed new lights on the characteristics of the hydrogen surface characteristics when it is stored in the subsurface reservoirs.

The structure of the paper is as follows. First, the experimental setup and procedure to measure the contact angle will be described in detail. Then the image processing methodology to measure the contact angles from the captured images is presented. In its following section, results and their relevance for UHS will be discussed. Finally, concluding remarks are presented.

2. Methods and materials

In this study, the Captive-Bubble method was utilized to measure intrinsic contact angles using a gas bubble at a solid-liquid interface. This method is advantageous over the alternative Sessile Drop method, because spreading and diffusion of the brine into porous hydrophilic substrates in the latter method poses experimental challenges, making the data less reliable (Prydatko et al., 2018).

2.1. Materials

Hydrogen with a purity of 99.99 mol%, produced by Lindegas, was used. The rock slabs were taken from a sawed homogeneous Bentheimer and Berea sandstone blocks. The properties of Bentheimer and Berea have been studied in literature (Peksa et al., 2015; Farajzadeh et al., 2017; Kapetas et al., 2015). The samples were mainly composed of quartz (95%)which was evenly distributed throughout the rock matrix (see appendix Figs. 10 and 11). The average porosity of the Bentheimer and Berea sandstones were about 20%, and permeability around 2 to 3, and 0.1 Darcy, respectively. Each slab had dimensions of $30 \times 6 \times 12$ mm. In addition to brine containing NaCl, a synthetic seawater (Laskaris, 2015) with the composition in Table 1 was also used in the experiments.

Table 1
Synthetic seawater composition.

Salt	Quantity (ppm)
NaCl	24,500
KCl	670
MgCl2.6H2O	10,150
CaCl2.2H2O	1450

2.2. Microscopic image analysis of rock samples

To quantify the surface roughness of rock slabs, 2D and 3D microscopic images were taken using a LEICA 3D stereo explorer Fig. 1. The surface profiles were characterized based on the internationally-recognized standard of EN ISO 287, where the so-called P_a factor defines the surface roughness (Kaveh et al., 2014). P_a is the arithmetic mean of the absolute ordinate height values Z(x) within a sampling length (l_p). The average roughnesses of the Bentheimer and Berea slabs have been measured 0.030 and 0.025 mm, respectively.

2.3. Experimental setup

The captive-bubble setup, modified after Kaveh et. al. (2014), was used to measure contact angles in the system of hydrogen/brine/rock at high pressures and temperatures. The schematic of the experimental setup is given in Fig. 2. The setup comprises of a single steel cell, which holds the rock sample and brine. The injection of the brine and other fluids takes place from the bottom and from different inlets. Extraction of the brine and gas from the cell was done from the top. The pressure in the cell was held constant by a back-pressure regulator connected to a large nitrogen cylinder. Injection of both brine and hydrogen was done with the use of two Vindum pumps. To bring the brine and hydrogen to equilibrium, a pressure gauge was installed in between the hydrogen pump and the cell. Hydrogen flows through a line with respective inner and outer diameters of 0.25 mm and 1.58 mm to a nozzle from which the hydrogen was released into the brine. The bubble that was created on the rock surface was photographed with a Canon 90 camera (with a maximum resolution of 12.3 MP) attached to an endoscope. The pressure and temperature of the setup were monitored continuously and recorded in a computer connected to the system.

2.4. Experimental procedure

To start the experiment the cell, including the rock sample, was initially filled with the brine over night to reach equilibrium. Then, at the desired pressure and temperature, a hydrogen bubble was injected through a needle at the bottom of the cell. Due to buoyancy, the bubble arises and sticks underneath of the rock sample. The pictures of the released bubbles were taken by using the connected digital camera through the endoscope at one side of the cell and diffusion of the

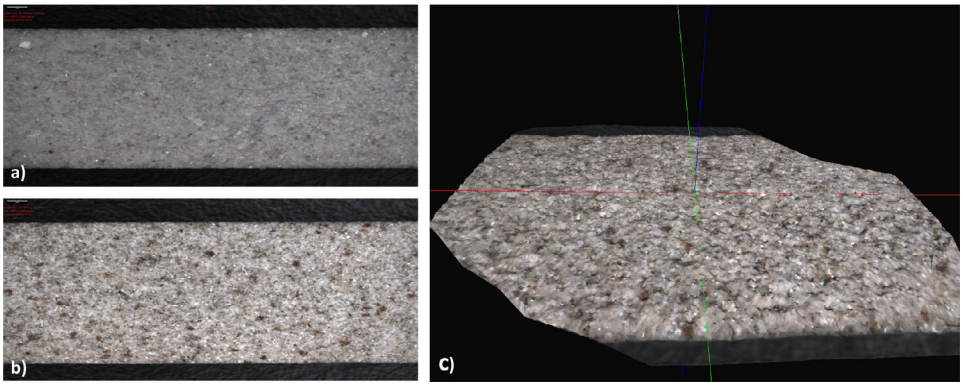

Fig. 1. Microscopic surface images: a) 2D-Bentheimer, b) 2D-Berea, and c) 3D-Berea.

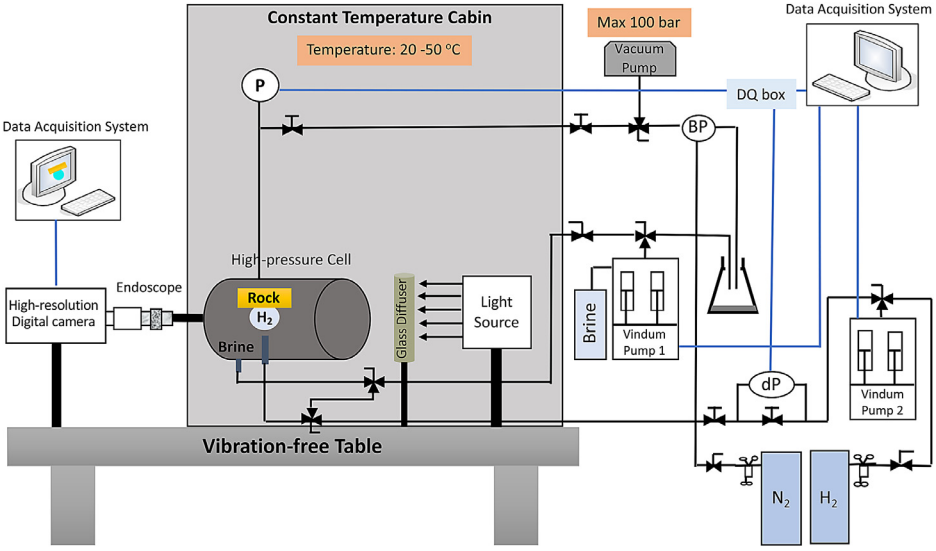

Fig. 2. Schematic of the captive-bubble cell experimental setup.

light source at the other side. To get sharp pictures of the bubbles, the resolution of imaging was set to 6.9 MP (3216×2136). Due to diffusion and dissolution of hydrogen into brine, the size of the bubbles changed over time. Consequently, several images were taken after injection of one bubble at each pressure and temperature. Therefore, for each experimental condition, the minimum and the maximum contact angles were reported in addition to the averaged values.

2.5. Image analysis

To calculate the contact angles, the captured images from the hydrogen bubbles were analyzed using an in-house MATLAB code. The needle diameter inside the cell was used to define the scale of the images. Afterwards, the image was converted to grey-scale format and was cropped to only keep the bubble and the rock surface. To find the boundary of the bubble, the image was subsequently binarized. Tracing boundary of the bubble and detecting the apex as well as contact points were followed by fitting the best curve based on the Axisymmetric Drop Shape Analysis-Profile (ADSA-P) technique (Li et al., 1992). All the main steps of the image analysis are shown in Fig. 4. The ADSA-P technique fits the best theoretical Laplacian curve on the physical observed bubble interface (Li et al., 1992). The Young-Laplace capillarity equation for two fluid phases is given as

$$\Delta P = \sigma(\frac{1}{R_1} + \frac{1}{R_2}), \tag{1}$$

where σ is interfacial tension, R_1 and R_2 are the two principle radii of the curvature. Because of the axisymmetry of the bubble in Eqn 1, the radii are considered equal at the apex ($R_1 = R_2 = R_0$), i.e.,

$$\Delta P_{apex} = \frac{2\sigma}{R_0}. \tag{2}$$

Also, by considering the gravity as the only external force across the interface, the pressure difference in Eqn 2 is assumed to be a linear function of the hydrostatic pressure ($\Delta\rho gz$) with interception of ΔP_0 at a reference plane, i.e.,

$$\Delta P = \Delta P_0 + \Delta\rho gz. \tag{3}$$

As shown in Fig. 3, the origin of the coordinate system was placed at the apex point. The x-axis is tangent to the origin and normal to the axis of symmetry. Therefore, Eqn 3 can be rewritten as

$$\sigma(\frac{1}{R_1} + \frac{sin(\theta)}{x}) = \frac{2\sigma}{R_0} + \Delta\rho gz, \tag{4}$$

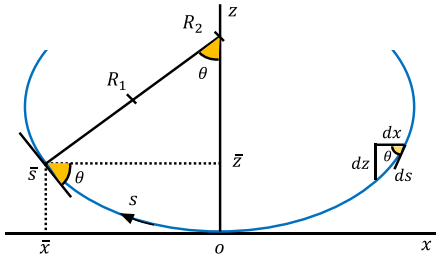

Fig. 3. Schematic of an axisymmetric drop, modified after Li et al. (1992).

where R_1 rotates in the plane of x-z and $R_2 = x/sin(\theta)$ rotates in the plane of z-y. Eqn 4 is restated as

$$\frac{dx}{ds} = cos\theta \tag{5}$$

$$\frac{dz}{ds} = sin\theta \tag{6}$$

$$\frac{d\theta}{ds} = \frac{2}{R_0} + \frac{\Delta\rho gz}{\sigma} - \frac{sin\theta}{x} \tag{7}$$

Eqn 5, 6, and 7 are first order differential equations in terms of the arc length (s). Finally, these three differential equations (i.e., Eqn 5, 6, and 7) are integrated using Runge-Kutta numerical approach to find theoretical Laplacian curve. In order to find the corresponding contact angle, the objective function is defined to minimize the deviation of the physically-observed curve from a theoretical curve by adjusting parameters: radius of the curvature at the apex, R_0 and interfacial tension, σ. The detail of this procedure has been extensively explained in the literature (Li et al., 1992). Brine and gas density were calculated based on the literature thermodynamic formulation for each specific pressure and temperature condition (Batzle and Wang, 1992) and reported in the appendix, Tables 10–15.

2.6. Calibration of the setup

Before starting the main test for the hydrogen gas, the setup was calibrated against the literature data for a nitrogen/brine/quartz system. The literature reports contact angle of nitrogen on a smooth alpha-quartz crystal surface at pressure of 13 MPa and temperature of 333K (Al-Yaseri et al., 2015). Under the same experimental conditions, the

Table 2
Summary of calibration of the setup with the literature data (Al-Yaseri et al., 2015) for nitrogen/brine/sandstone.

Parameters	Literature test (Al-Yaseri et al., 2015)	Our test
Liquid phase	5000 ppm NaCl	5000 ppm NaCl
Gas phase	N_2	N_2
Rock sample	Smooth alpha-quartz crystal surface	Bentheimer (~95% quartz)
Pressure (bar)	130	130
Temperature (°C)	60	60
Contact angle (°)	40.6 ±3.9	40.8 ±5.9

method used in our study (i.e., captive-bubble method), resulted in the contact angle of (40.8° ±5.9°) for nitrogen/brine/Bentheimer sandstone system, which is in close agreement with the reported data (Al-Yaseri et al., 2015), i.e, 40.6° ±3.9°. Summary of the validation test is provided in Table 2.

2.7. Summary of the test cases

Extensive experiments were conducted to examine the effect of pressure, temperature, salinity, and rock type on the contact angle in the hydrogen/brine/sandstone system. The experimental conditions are summarized in Fig. 5.

3. Results and discussion

In this section the results of the experiments will be explained in detail. The impact of each parameter, i.e., pressure, temperature, salinity, rock type will be separately discussed. Note that, in order to prove reproducibility of the results, measurements were repeated up to three times (see appendix Table 16-17-–18).

3.1. Effect of bubble size on the contact angle

As shown in Fig. 6, it was noticed that due to dissolution/diffusion of the hydrogen gas into brine, the size of the created bubbles continuously decreased during the experiments until they disappeared. Interestingly, as the size of the bubble decreases, the calculated contact angle increases. A similar behavior has been reported by Kaveh et. al. (2014), Haeri et al. (2020), and Jung et al., (2012) for CO_2/brine/rock system. Therefore, to capture the effect of the bubble size on the reported contact angles, for each test case, several images were taken from every injected bubble at different times, out of which only four images were analyzed to calculate the minimum, maximum, and the mean contact angle. The mean contact angle is the arithmetic average of the four measured contact angles. An example is given in Fig. 6a, which results in the contact angles shown in Fig. 6b.

3.2. Test Case 1: Effect of pressure and temperature

Fig. 7 shows the effect of different pressures and temperatures on the contact angles of the hydrogen/water/Bentheimer system in the absence and presence of NaCl (5000ppm). No obvious correlation was found, as all the data points fall within the accuracy range of the conducted experiments. Detailed results are given in Tables 3–4.

3.3. Test Case 2: Effect of salinity

To quantify the impact of salinity, brines with three different salinities, i.e., 0, 5000 and 50,000 ppm NaCl were used at a constant temperature of 30 °C and four different pressures in the range of 20

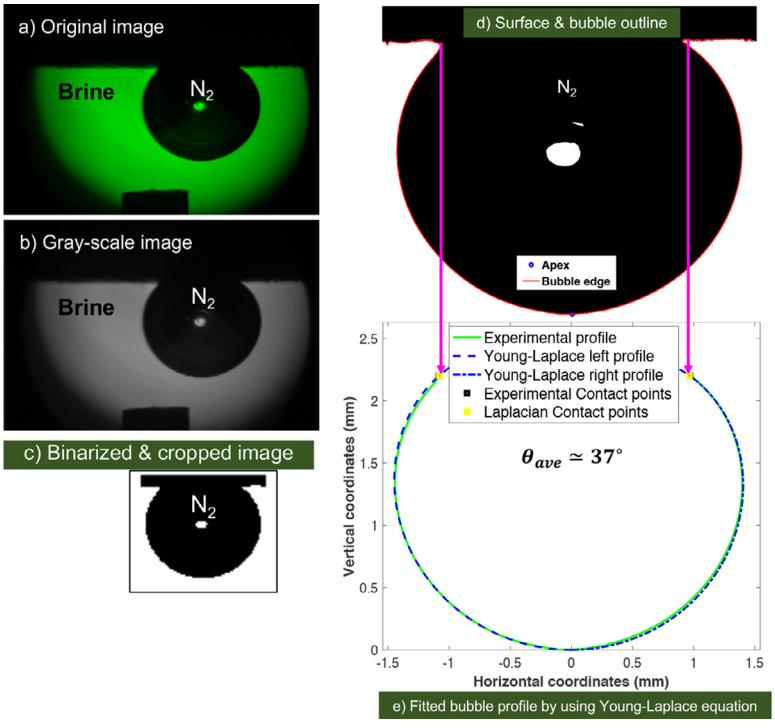

Fig. 4. The image processing procedure.

Table 3
Contact angle values of hydrogen/pure water/Bentheimer.

Test No.	Temp. (°C)	Press. (bar)	θ_{ave} (°)	θ_{range} (°)	Vol.$_{ave}$ (mm^3)	Vol.$_{range}$ (mm^3)
1 T~20°C	22.3	20.3	30	[28.7, 32.8]	4.56	[2.36, 7.05]
	23.5	50.2	32.6	[29.2, 39.1]	5.49	[1.34, 9.96]
	23.4	70.7	31.1	[25.9, 37.8]	3.93	[1.45, 9.10]
	23.9	100.5	30	[26.0, 36.9]	4.05	[1.48, 7.36]
2 T~30°C	31.9	22	33.7	[30.6, 37.1]	3.48	[2.21, 4.66]
	32.5	51.8	30.5	[29.4, 32.9]	3.09	[2.20, 3.66]
	32.8	71.5	33.9	[32.6, 36.5]	3.39	[2.38, 4.48]
	33.2	100.5	31.7	[29.0, 39.0]	5.27	[1.93, 9.49]
3 T~40°C	39.5	20.3	31.9	[29.0, 35.3]	5.09	[2.61, 8.38]
	39.9	50.2	29.8	[26.3, 35.9]	7.42	[2.21, 12.67]
	40.1	72.8	31.2	[28.9, 36.0]	7.04	[2.27, 12.58]
	40.3	100.3	32	[28.9, 35.2]	3.91	[2.32, 6.02]
4 T~50°C	49.1	19.8	28.4	[26.1, 29.2]	7.42	[3.96, 10.65]
	49.2	50.6	33.2	[29.4, 39.3]	4.7	[1.68, 8.39]
	49.3	70.2	29.8	[28.6, 31.2]	4.41	[2.66, 6.33]
	49.3	101.2	32.8	[29.9, 38.0]	4.12	[2.14, 6.35]

Table 4
Contact angle values of hydrogen/brine (5000 ppm NaCl)/Bentheimer.

Test No.	Temp. (°C)	Press. (bar)	θ_{ave} (°)	θ_{range} (°)	Vol.$_{ave}$ (mm^3)	Vol.$_{range}$ (mm^3)
1 T~20°C	21.3	20	33.1	[30.0, 39.2]	3.99	[1.62, 6.14]
	22.1	51.9	29.1	[26.8, 32.8]	4.08	[1.82, 6.53]
	22.3	71.5	33.5	[29.3, 40.5]	3.76	[1.28, 6.50]
	22.9	100.5	33.9	[29.7, 42.7]	4.13	[1.01, 7.37]
2 T~30°C	38.9	21	29.5	[28.7, 30.5]	4.61	[2.67, 6.55]
	32.2	49.9	34.9	[30.8, 42.2]	3.42	[1.21, 5.77]
	32.7	71.1	36	[32.8, 41.6]	2.8	[1.19, 4.72]
	33.1	98.9	31.9	[31.1, 34.1]	5.59	[2.08, 11.13]
3 T~40°C	38.9	19.6	32.7	[30.7, 36.0]	4.33	[2.45, 6.32]
	39.5	50.8	34.1	[30.5, 40.7]	3.91	[1.44, 6.48]
	39.9	69.9	34.3	[29.4, 43.0]	4.06	[1.16, 7.18]
	40.1	100.1	37.3	[34.0, 41.3]	2.24	[1.34, 3.22]
4 T~50°C	47.4	20.7	33.6	[29.2, 40.2]	4.48	[1.51, 7.78]
	48.3	51.3	33.6	[29.9, 41.4]	4.03	[1.40, 6.45]
	49	70.6	34.2	[30.0, 41.5]	4.34	[1.50, 7.91]
	49.2	100.7	33.7	[29.9, 41.6]	5.7	[1.31, 12.66]

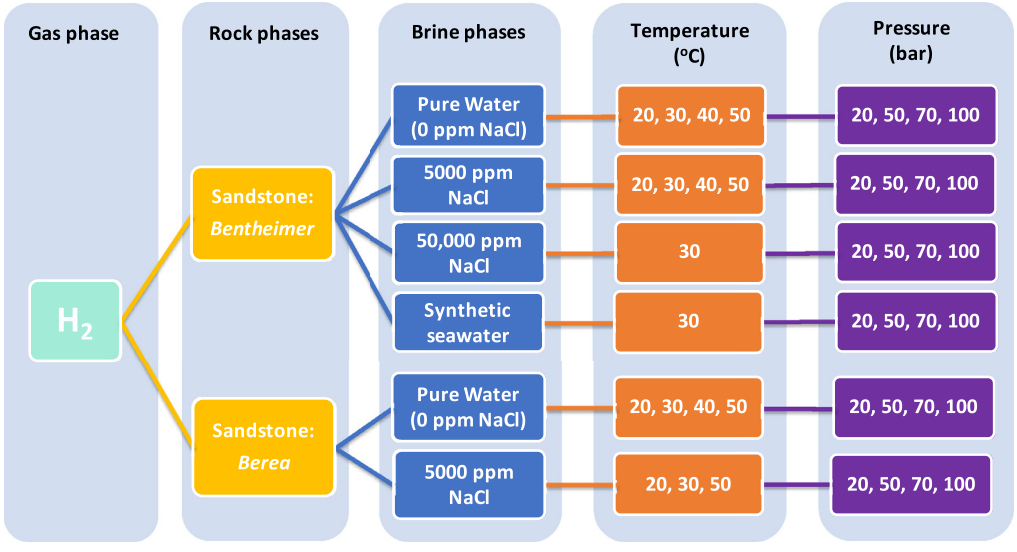

Fig. 5. Experimental conditions for hydrogen tests.

to 100 bar. The results are shown in Fig. 8. The change of salinity did not result in a meaningful change in the measured contact angles, indicating that the wetting state of the rock was insensitive to salinity in the presence of hydrogen. Detailed results for salinity of 50,000 ppm NaCl and seawater are also provided in Tables 5 and 6.

3.4. Test Case 3: Effect of rock type

Fig. 9 shows the effect of rock type on the contact angles of the hydrogen/pure water/rock system with Bentheimer and Berea sandstones. No obvious correlation was found, as all the data points fall within the accuracy range of the conducted experiments. Detailed results are given

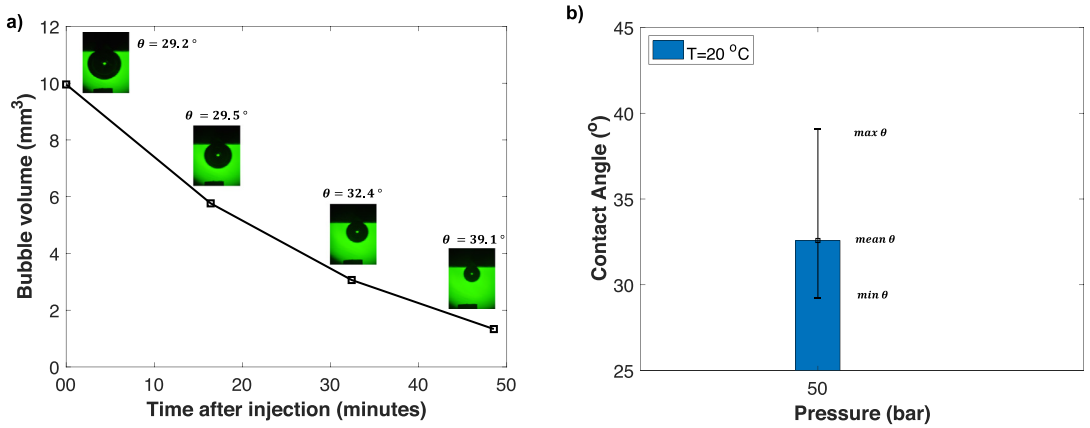

Fig. 6. Effect of bubble size in the system of hydrogen/water/Bentheimer at 23.5°C and 51.2 bar: a) Volume changes over time, b) Corresponding reported range of contact angles.

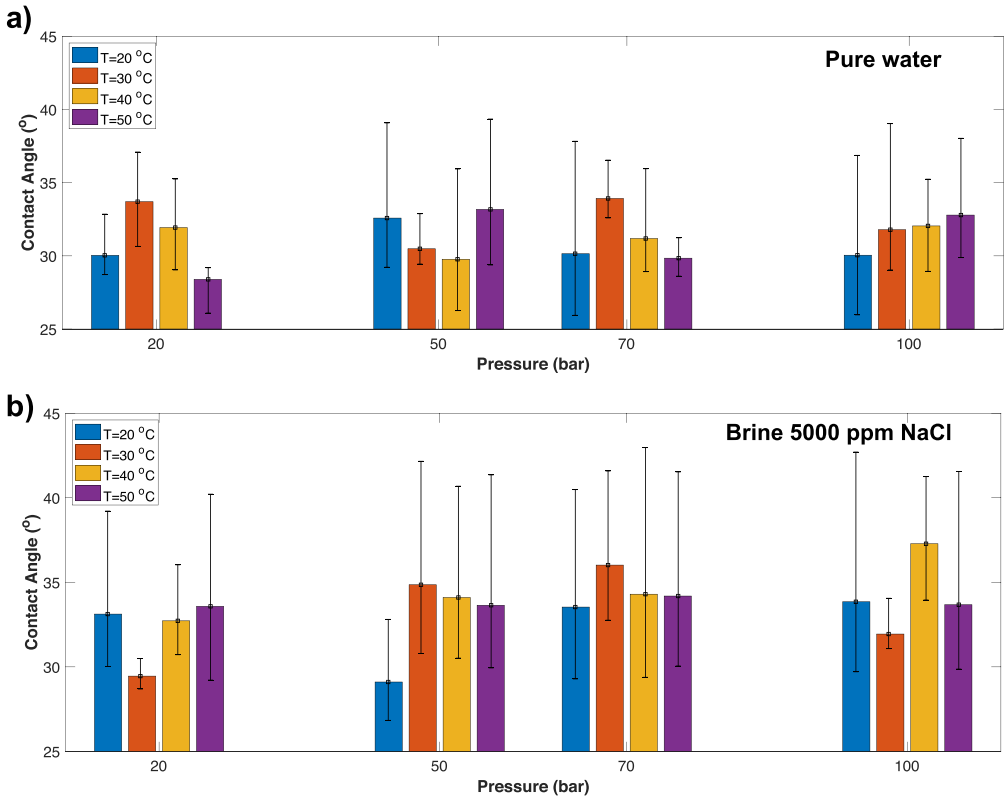

Fig. 7. Effect of pressure and temperature in the system of hydrogen/brine/Bentheimer at 20, 30, 40 and 50 °C and 20, 50, 70 and 100 bar, a) pure water and b) brine with 5000 ppm NaCl.

in Tables 3 and 7. To confirm repeatability of the tests, the results of the repeated experiments are reported in Tables 16, 17, 18 and 19 in the appendix.

4. Conclusions and outlook

Wettability of the rock in contact with brine and hydrogen plays a crucial role in the displacement processes in UHS. This paper reports experimental measurements of the contact angle of the hydrogen/brine/sandstone system, relevant for underground hydrogen storage. This is the first step in understanding and quantifying the impact of different parameters in accurate prediction of the fate of stored and produced hydrogen. The captive-bubble method was used for measuring contact angle. To ensure accurate measurements, the setup was successfully calibrated against the existing literature data with nitrogen gas. Then, through several test cases, the intrinsic contact angles were measured under various experimental conditions. It was found that, under our experimental conditions and within the accuracy of the method and setup, the contact angles in the examined systems were not affected by temperature, pressure and salinity. Under all conditions, the presence of hydrogen did not appear to affect the wettability of the Bentheimer sandstone. All the results indicated water-wet conditions with contact angles in the range of 21.1° to 43°. This general conclusion and contact angles of less than 50° agree well with the conclusions of literature (Yekta, Manceau, Gaboreau, Pichavant, Audigane, 2018). A major discrepancy between our data and the data reported

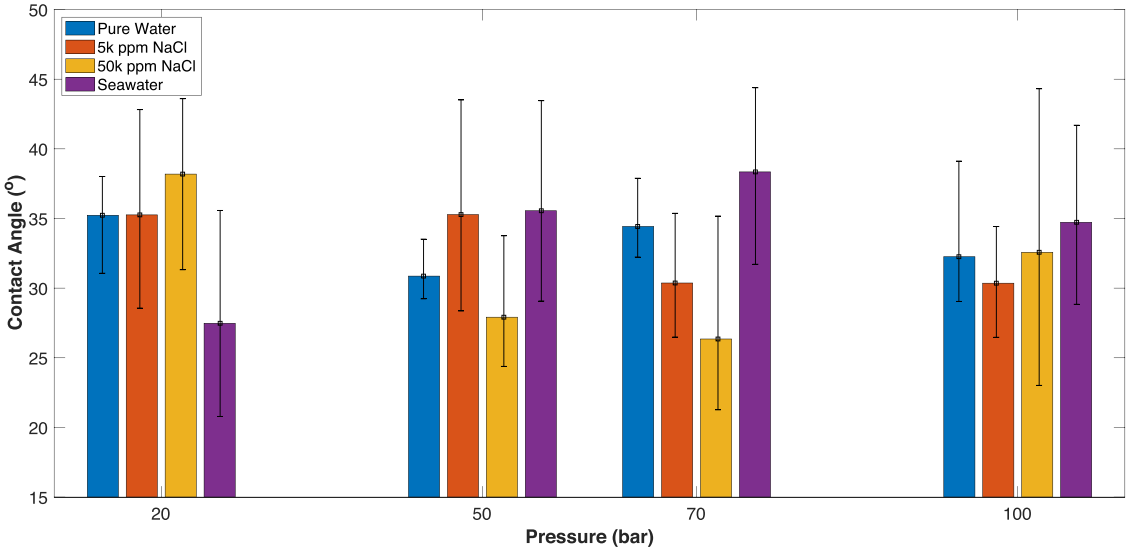

Fig. 8. Effect of salinity in the systems of hydrogen/brine/Bentheimer using pure water, brine (5000 ppm NaCl), brine (50,000 ppm NaCl), and seawater at about 30 °C for four pressure values of 20, 50, 70, 100 bar.

Table 5
Contact angle values of hydrogen/brine (50,000 ppm NaCl)/Bentheimer.

Test No.	Temp. (°C)	Press. (bar)	θ_{ave} (°)	θ_{range} (°)	$Vol._{ave}$ (mm^3)	$Vol._{range}$ (mm^3)
1 T~30°C	31.3	21.1	33.3	[30.4, 36.6]	4.02	[2.10, 6.49]
	31.9	51.4	32.8	[30.3, 37.5]	3.54	[1.66, 5.34]
	33	70.6	31.6	[29.1, 36.7]	3.31	[1.53, 5.38]
	33.3	100.7	34.5	[29.8, 42.5]	3.84	[1.36, 5.77]

Table 6
Contact angle values of hydrogen/brine (synthetic seawater) /Bentheimer.

Test No.	Temp. (°C)	Press. (bar)	θ_{ave} (°)	θ_{range} (°)	$Vol._{ave}$ (mm^3)	$Vol._{range}$ (mm^3)
1 T~30°C	31.0	20.5	27.47	[20.8, 35.6]	5.61	[2.62, 8.72]
	31.3	50.2	35.5	[29.1, 43.5]	1.4	[0.42, 2.64]
	31.6	69.6	38.3	[31.7, 44.4]	1.38	[0.61, 2.09]
	31.6	100.7	34.7	[28.8, 41.7]	2.61	[1.11, 4.42]

Table 7
Contact angle values of hydrogen/pure water/Berea.

Test No.	Temp. (°C)	Press. (bar)	θ_{ave} (°)	θ_{range} (°)	$Vol._{ave}$ (mm^3)	$Vol._{range}$ (mm^3)
1 T~20°C	23.6	20.8	30.4	[27.5, 34.9]	4.96	[1.14, 9.19]
	23.5	50.6	29	[26.8, 34.5]	5	[0.96, 10.74]
	23.7	70.2	29.1	[25.2, 33.3]	5.22	[1.04, 10.28]
	23.9	100.7	29.6	[23.6, 41.9]	4.17	[0.33, 9.51]
2 T~30°C	32.6	19.4	26.1	[23.3, 29.2]	7.65	[1.36, 15.81]
	32.7	50	23.6	[21.1, 27.9]	7.28	[0.79, 14.17]
	32.8	69.3	31.2	[27.9, 36.1]	3.38	[0.54, 7.29]
	33	101.1	31.7	[28.3, 39.3]	3.61	[0.45, 8.59]
3 T~40°C	38.6	21.2	31.1	[27.3, 34.3]	3.01	[0.95, 5.64]
	38.6	51	29.5	[25.1, 34.8]	4.34	[0.94, 9.68]
	38.6	69.4	29.4	[27.4, 32.5]	3.56	[1.17, 7.14]
	38.9	100.7	28.9	[25.8, 31.6]	4.98	[1.52, 10.35]
4 T~50°C	47.6	20.5	27	[25.6, 30.5]	5.57	[0.91, 10.51]
	47.8	49.4	26.4	[23.2, 31.4]	6.49	[0.93, 14.03]
	48.2	70.6	30.1	[29.4, 31.5]	6.68	[5.13, 8.52]
	48.2	99.7	30.5	[27.2, 35.3]	4.55	[0.91, 9.80]

by Iglauer et al. (2021) is the absence of a general trend between the parameters (pressure, temperature and salinity) and the measured contact angles. This can be attributed to the differences in the measurement methods, experimental conditions, and sample preparation. It was also observed that the bubble size affects the calculated contact angle values due to dominance of gravity for the larger gas bubbles, and possibly different surface composition of the rock.

The presented experimental data and images are all made digitally available open-source at https://gitlab.tudelft.nl/ADMIRE_Public/PoreScale_H2 repository.

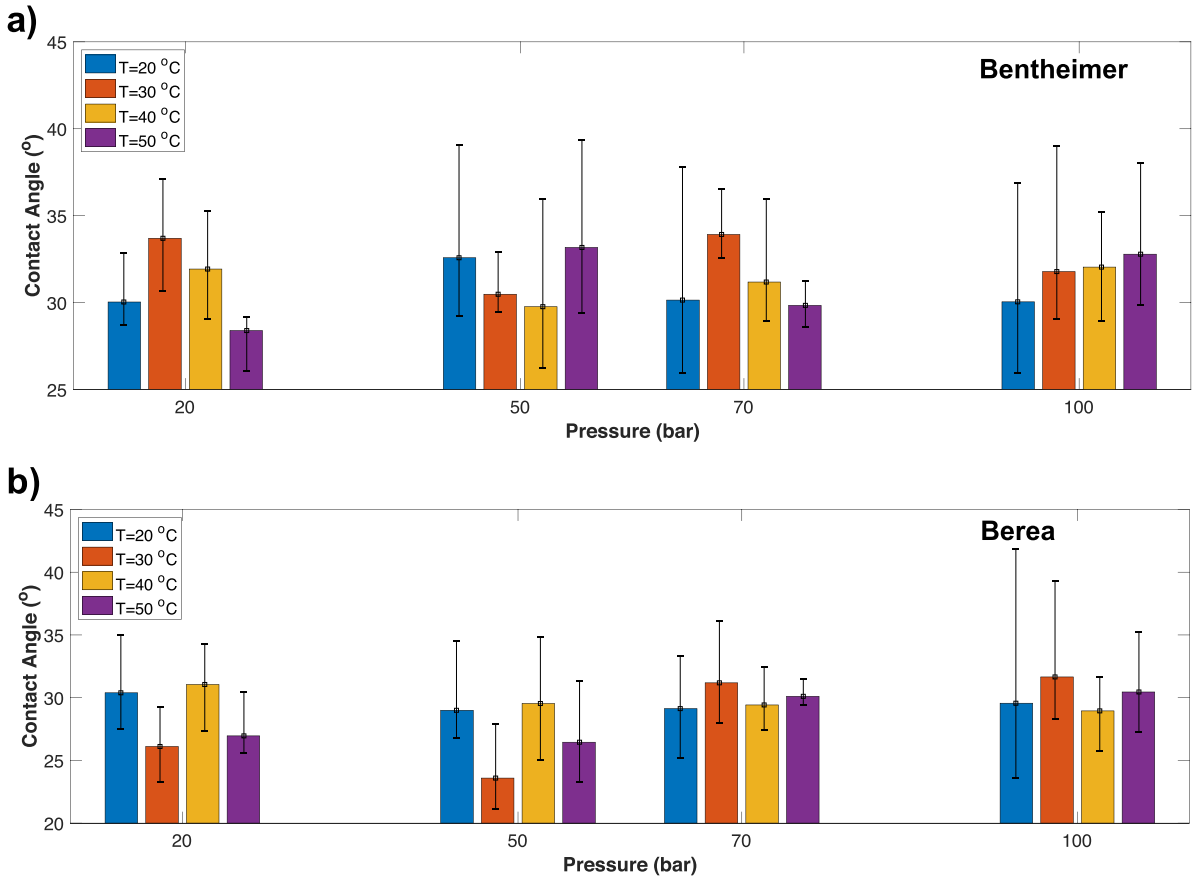

Fig. 9. Effect of rock type in the system of hydrogen/pure water/rock at 20, 30, 40 and 50 °C and 20, 50, 70 and 100 bar, a) Bentheimer and b) Berea.

Appendix

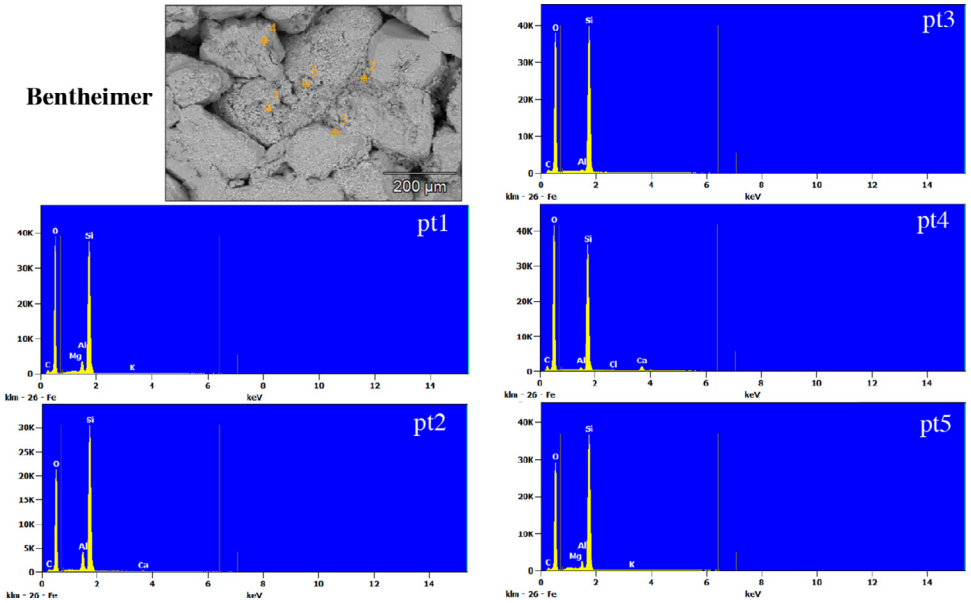

Fig. 10. SEM data of Bentheimer sandstone.

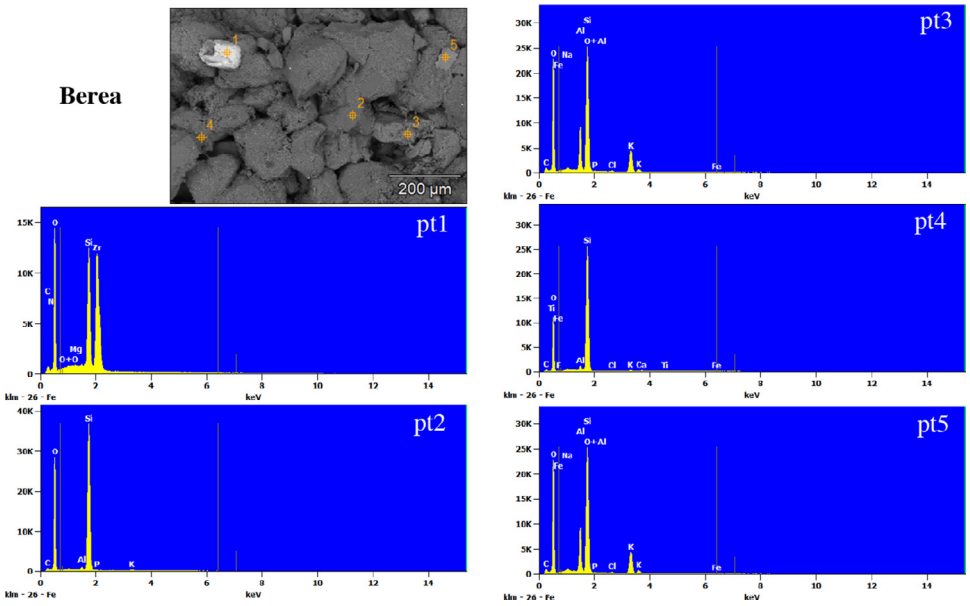

Fig. 11. SEM data of Berea sandstone.

Table 8
Review of literature experimental measurement of contact angles for systems containing Gas/Brine/Rock.

Reference	Substrate	Fluids	Gases	Method	P & T conditions	Comments	Wettability
Yang et al. (2008)	Carbonate Weyburn limestone	Weyburn brine	CO_2	Sessile-Drop ADSA	0.1–31.6 MPa; 300 & 331 K	θ increases with P, θ decreases with T limestone	intermediate wet 27°C (45–100)° 58°C (88–135)°
Espinoza and Santamarina, (2010)	Carbonate, Calcite Sandstone, Quartz, oil-wet Quartz PTFE	water, NaCl, 200 g/l	CO_2	Sessile-Drop ADSA	up to 20 MPa; 298 K	θ increases with P, on nonwetting surfacs: PTFE & oil-wet Quartz θ slightly decreases in water-wet Quartz & Calcite surfaces, θ increases with salinity	strongly water-wet Calcite: 20° Quartz: 20° Oil-wet Quartz: 85–90° PTFE: 100–140°
Bikkina, (2011)	Carbonate, Calcite; Sandstone, Quartz	water	CO_2	Sessile-Drop	1.3–21 MPa; 298–323 K	θ increases with P slightly then decreases slightly and remains fairly constant	weakly water-wet
Mills et al. (2011)	Carbonate, Calcite Sandstone, Quartz Biotite Orthoclase Labradorite	Brine	CO_2 N_2	Captive-Bubble	6 MPa & 295 K; 13 MPa & 313 K	θ increases with P slightly	strongly water-wet
Broseta et al. (2012)	Carbonate Calcite	NaCl, 4g/l	CO_2	Captive-Bubble	0.5–14 MPa; 308 K	θ increases with P	weakly water-wet
	Rousse caprock (70% Calcite)	NaCl, 4g/l, 40g/l, 350g/l	CO_2	Captive-Bubble	1.1–15.5 MPa; 3.8–413 K	θ remains constant with P, θ increases with salinity	strongly to weakly water-wet
Jung and Wan (2012)	Sandstone and Silica	water,brine 5M	CO_2	Captive-Bubble;Sessile-Drop;No difference in results	0.1–25 MPa & 318 K;20 MPa & 323 K	θ increases with P in: 7–10 MPa, after 10 MPaθ remains constant θ increases with salinity linearly	stronglywater-wet
Wang et al. (2013)	Carbonate and Calcite	water, Synthetic brines	CO_2	Captive-Bubble	7 MPa & 303 K; 20 MPa & 323 K	θ increases with P slightly, θ decreases with salinity	strongly water-wet

Table 9
Review of literature experimental measurement of contact angles for systems containing Gas/Brine/Rock (continue).

Reference	Substrate	Fluids	Gases	Method	P & T conditions	Comments	Wettability
Farokhpoor et al. (2013)	Carbonate Calcite Sandstone Quartz feldspar Mica	water, NaCl, 0.2 &0.8 M	CO_2	Captive-Bubble	0.1–40 MPa; 309 K	θ increases with P on Mica for the rest not significant changes θ increases with T on Quartz	strongly water-wet
Kaveh et al. (2014)	Sandstone Bentheimer	water	CO_2 CO_2+N_2	Captive-Bubble ADSA	0.2–15 MPa; 318 K	not significant changes with P	water-wet
Andrew et al. (2014)	Carbonate Ketton limestone (99% Calcite)	KI, 7 wt%	CO_2	Pore-Scale microCT	10 MPa; 323 K		weakly water-wet
Al-Yaseri et al. (2015)	Sandstone Quartz	water, NaCl, 0.5 wt%	CO_2 N_2 CO_2+N_2	Sessile-Drop	13 MPa; 333 K		47° 40.6° 33.9°
Arif et al. (2017)	Carbonate Calcite	water, NaCl, 0–20 wt%	CO_2	Tiltting-Plate	0.1–20 MPa; 308–343 K	θ increases with P & salinity θ decreases with T & roughness	strongly to weakly water-wet
Stevar et al. (2019)	Carbonate Calcite	NaHCO3 (aq), 1 mol/kg	CO_2	Sessile-Drop Titling plate	up to 30 MPa; 298–373 K	θ increases up to 10 MPa, after 10 MPa θ decreases, and being constant θ decreases with T & roughness	water-wet intermediate-wet
Haeri et al. (2020)	Sandstone Navajo Nugget Bentheimer Bandera Brown Berea Mt. Simon	NaHCO3 (aq), 1 mol/kg	CO_2	Captive-Bubble		No clear trend with P & T	strongly to weakly water-wet
Iglauer et al. (2021)	Sandstone Quartz and aged Quartz, in acid	NaCl, 10 wt%	H_2	Sessil-Drop Tilting plate	0.1–25 MPa, 296–343 K	θ increases with P & T	water-wet less than 50°, for aged surface: intermediate-wet

Table 10
Density of water and hydrogen phases used for contact angle measurement of hydrogen/pure water/Bentheimer tests.

Temp. (°C)	Press. (bar)	ρ_w(kg/m^3)	ρ_{H_2}(kg/m^3)
22.3	20.3	997.51	1.65
23.5	50.2	998.57	3.98
23.4	70.7	999.51	5.55
23.9	100.5	1000.71	7.73
24.4	23.5	997.16	1.89
24.5	50.7	998.35	4.01
25.0	70.4	999.11	5.49
25.1	100.7	1000.42	7.72
31.9	22.0	995.12	1.73
32.5	51.8	996.25	3.99
32.8	71.5	997.01	5.44
33.2	100.5	998.15	7.51
39.5	20.3	992.68	1.56
39.9	50.2	993.83	3.78
40.1	72.8	994.73	5.41
40.3	100.3	995.84	7.33
38.8	20.7	992.93	1.59
39.0	48.8	994.08	3.69
39.4	70.6	994.88	5.26
39.5	99.2	996.07	7.27
49.1	19.8	989.17	1.47
49.2	50.6	990.44	3.70
49.3	70.2	991.23	5.08
49.3	101.2	992.53	7.20

Table 11
Density of brine and hydrogen phases used for contact angle measurement of hydrogen/brine (5000 ppm NaCl)/Bentheimer tests.

Temp. (°C)	Press. (bar)	ρ_w(kg/m^3)	ρ_{H_2}(kg/m^3)
21.3	20.0	1000.91	1.63
22.1	51.9	1002.16	4.13
22.3	71.5	1002.99	5.63
22.9	100.5	1004.14	7.76
24.0	20.3	1000.29	1.64
24.8	49.4	1001.39	3.91
24.7	70.9	1002.37	5.54
24.4	100.9	1003.77	7.75
31.7	21.0	998.24	1.65
32.2	49.9	999.36	3.85
32.7	71.1	1000.13	5.41
33.1	98.9	1001.21	7.40
38.9	19.6	995.91	1.51
39.5	50.8	997.05	3.83
39.9	69.9	997.73	5.20
40.1	100.1	998.95	7.32
38.7	20.4	996.02	1.57
39.0	51.1	997.24	3.86
39.2	70.1	997.98	5.23
39.4	100.4	999.20	7.36
47.4	20.7	992.88	1.55
48.3	51.3	993.82	3.76
49.0	70.6	994.35	5.11
49.2	100.7	995.53	7.16

Table 12
Density of brine and hydrogen phases used for contact angle measurement of hydrogen/brine (50,000 ppm NaCl)/Bentheimer tests.

Temp. (°C)	Press. (bar)	ρ_w(kg/m^3)	ρ_{H_2}(kg/m^3)
31.3	21.1	1004.18	1.66
31.9	51.4	1004.82	3.97
33.0	70.6	1004.43	5.37
33.3	100.7	1005.37	7.52

Table 13
Density of brine and hydrogen phases used for contact angle measurement of hydrogen/synthetic seawater/Bentheimer tests.

Temp. (°C)	Press. (bar)	ρ_w(kg/m^3)	ρ_{H_2}(kg/m^3)
31	20.5	1006.82	1.61
31.3	50.2	1007.89	3.88
31.6	69.6	1008.51	5.32
31.6	100.9	1009.85	7.57

Table 14
Density of water and hydrogen phases used for contact angle measurement of hydrogen/pure water/Berea tests.

Temp. (°C)	Press. (bar)	ρ_w(kg/m^3)	ρ_{H_2}(kg/m^3)
23.6	20.8	997.23	1.68
23.5	50.6	998.59	4.01
23.7	70.2	999.42	5.50
23.9	100.7	1000.72	7.75
24.0	20.7	997.13	1.67
23.7	50.7	998.55	4.02
23.5	71.5	999.52	5.60
23.5	100.8	1000.82	7.77
22.4	19.7	997.46	1.60
22.8	49.1	998.69	3.91
32.6	19.4	994.80	1.52
32.7	50.0	996.11	3.85
32.8	69.3	996.92	5.28
33.0	101.1	998.24	7.56
38.6	21.2	993.02	1.63
38.6	51.0	994.30	3.85
38.6	69.4	995.09	5.19
38.9	100.7	996.33	7.39
47.6	20.5	989.78	1.53
47.8	49.4	990.93	3.63
48.2	70.6	991.68	5.12
48.2	99.7	992.90	7.12

Table 15
Density of brine and hydrogen phases used for contact angle measurement of hydrogen/brine (5000 ppm NaCl)/Berea tests.

Temp. (°C)	Press. (bar)	ρ_w(kg/m^3)	ρ_{H_2}(kg/m^3)
21.6	20.2	1000.85	1.64
21.8	50.6	1002.17	4.04
22.3	70.2	1002.93	5.53
22.6	100.2	1004.20	7.74
32.4	21.6	998.06	1.69
32.4	50.6	999.33	3.90
32.5	71.4	1000.21	5.44
32.5	98.7	1001.39	7.40
47.3	21.6	992.95	1.61
47.7	49.6	993.98	3.65
48.1	69.9	994.68	5.07
48.5	99.6	995.77	7.10

Table 16
Contact angle values of hydrogen/pure water/Bentheimer, repeated tests.

Test No.	Temp. (°C)	Press. (bar)	θ_{ave} (°)	θ_{range} (°)	Vol.$_{ave}$ (mm^3)	Vol.$_{range}$ (mm^3)
1 T~20°C	24.4	23.5	33.7	[30.5, 38.8]	4.88	[1.99, 8.23]
	24.5	50.7	34.8	[30.3, 42.7]	4.05	[1.21, 7.10]
	25	70.4	37.5	[33.4, 44.4]	2.75	[0.96, 4.41]
	25.1	100.7	36.4	[32.4, 41.8]	3.91	[1.29, 8.37]
2 T~40°C	38.8	20.7	35.3	[31.5, 42.8]	3.92	[1.30, 6.64]
	39	48.8	35.3	[32.4, 41.6]	4.21	[1.41, 7.64]
	39.4	70.6	31.1	[27.3, 34.9]	4.47	[1.79, 8.59]
	39.5	99.2	36.2	[31.6, 42.3]	3.58	[1.15, 7.22]

Table 17
Contact angle values of hydrogen/brine (5000 ppm NaCl)/Bentheimer, repeated tests.

Test No.	Temp. (°C)	Press. (bar)	θ_{ave} (°)	θ_{range} (°)	Vol.$_{ave}$ (mm^3)	Vol.$_{range}$ (mm^3)
1 T~20°C	24	20.3	33.7	[29.7, 40.4]	3.92	[1.53, 5.56]
	24.8	49.4	35.6	[30.8, 42.6]	3.63	[1.18, 6.79]
	24.7	70.9	35.9	[30.5, 43.1]	3.45	[1.08, 5.97]
	24.4	100.9	32.4	[29.5, 37.5]	4.33	[1.54, 7.46]
2 T~40°C	38.7	20.4	31.3	[30.1, 33.3]	4.06	[2.41, 5.91]
	39	51.1	31.69	[27.4, 35.5]	3.89	[1.78, 6.27]
	39.2	70.1	37.4	[34.5, 40.3]	2.54	[1.32, 3.90]
	39.4	100.4	33.6	[30.5, 38.6]	3.51	[1.18, 6.43]

Table 18
Contact angle values of hydrogen/pure water/Berea, repeated tests.

Test No.	Temp. (°C)	Press. (bar)	θ_{ave} (°)	θ_{range} (°)	Vol.$_{ave}$ (mm^3)	Vol.$_{range}$ (mm^3)
1 T~20°C	24	20.7	30.5	[26.4,38.6]	5.17	[0.71,10.29]
	23.7	50.7	29.3	[25.3, 37.5]	5.35	[0.57, 12.05]
	23.5	71.5	26.6	[22.7, 32.8]	5.93	[0.76, 13.08]
	23.5	100.8	24.2	[22.2, 26.5]	9.68	[1.34, 17.42]
2 T~20°C	22.4	19.7	22.8	[20.76, 25.06]	8.66	[2.16, 16.84]
	22.8	49.1	26.4	[23.44, 29.44]	6.02	[1.05, 11.97]

Table 19
Contact angle values of hydrogen/brine (5000 ppm NaCl)/Berea.

Test No.	Temp. (°C)	Press. (bar)	θ_{ave} (°)	θ_{range} (°)	Vol.$_{ave}$ (mm^3)	Vol.$_{range}$ (mm^3)
1 T~20°C	21.6	20.2	27.2	[23.3,30.9]	6.91	[2.86,11.48]
	21.8	50.6	28.7	[25.3,31.8]	6.74	[1.41,15.52]
	22.3	70.2	29.6	[25.6,33.3]	5.21	[0.97,12.11]
	22.6	100.2	27.5	[25.3,30.1]	3.59	[2.15,5.03]
2 T~30°C	32.4	21.6	27.1	[25.1,28.3]	7.21	[3.05,11.91]
	32.4	50.6	27.8	[23.5,31.7]	5.99	[1.57,11.15]
	32.5	71.4	28	[23.7,31.2]	4.19	[1.18,8.15]
	32.5	98.7	27.9	[26.0,30.9]	5.05	[1.22,9.11]
4 T~50°C	47.3	21.6	30.4	[26.5,33.2]	4.71	[2.63,6.96]
	47.7	49.6	29.1	[26.6,33.7]	4.3	[0.94,7.79]
	48.1	69.9	27.3	[19.9,34.5]	3.88	[1.04,7.37]
	48.5	99.6	29.3	[26.6,33.7]	4.86	[0.88,10.18]

Declaration of Competing Interest

The authors declare that they have no known competing financial interests or personal relationships that could have appeared to influence the work reported in this paper.

CRediT authorship contribution statement

Leila Hashemi: Methodology, Writing - original draft. **Wuis Glerum:** Formal analysis, Data curation. **Rouhi Farajzadeh:** Methodology, Writing - review & editing, Supervision. **Hadi Hajibeygi:** Conceptualization, Methodology, Writing - review & editing, Supervision, Funding acquisition.

Acknowledgements

Hadi Hajibeygi was sponsored by Dutch National Science Foundation (NWO) under Vidi Project "ADMIRE" (grant number 17509). We thank ADMIRE user committee for allowing us publish this paper. Groups members of DARSim (Delft Advanced Reservoir Simulation) and ADMIRE (Adaptive Dynamic Multiscale Integrated Reservoir Earth) are acknowledged for fruitful discussions during the development of this work. This study was conducted in the Laboratory of Geoscience and Engineering at Delft University of Technology. We gratefully thank the technical staff of the Laboratory, specially Michiel Slob. Hossein Safari is also thanked for his help regarding the image processing code.

References

Al-Yaseri, A., Sarmadivaleh, M., Saeedi, A., Lebedev, M., Barifcani, A., Iglauer, S., 2015. N2 + co2 + nacl brine interfacial tensions and contact angles on quartz at co2 storage site conditions in the gippsland basin, victoria/australia. J. Petrol. Sci. Eng. 129, 58–62. https://doi.org/10.1016/j.petrol.2015.01.026.

Andrew, M., Bijeljic, B., Blunt, M.J., 2014. Pore-scale contact angle measurements at reservoir conditions using x-ray microtomography. Adv. Water Resour. 68, 24–31.

Arif, M., Lebedev, M., Barifcani, A., Iglauer, S., 2017. Co2 storage in carbonates: wettability of calcite. Int. J. Greenhouse Gas Control 62, 113–121.

Batzle, M., Wang, Z., 1992. Seismic properties of pore fluids. Geophysics 57 (11), 1396–1408. https://doi.org/10.1190/1.1443207.

Berg, S., Røcker, M., Ott, H., Georgiadis, A., van der Linde, H., Enzmann, F., Kersten, M., Armstrong, R., de With, S., Becker, J., Wiegmann, A., 2016. Connected pathway relative permeability from pore-scale imaging of imbibition. Adv. Water Resour. 90, 24–35. https://doi.org/10.1016/j.advwatres.2016.01.010.

Bikkina, Prem Kumar, 2011. Contact angle measurements of CO_2–water–quartz/calcite systems in the perspective of carbon sequestration. Int. J. Greenh. Gas Control 5, 1259–1271. https://doi.org/10.1016/j.ijggc.2011.07.001.

Blunt, M.J., 2017. Multiphase flow in permeable media: A Pore-Scale perspective. Cambridge University Press. https://doi.org/10.1017/9781316145098.

Broseta, D., Tonnet, N., Shah, V., 2012. Are rocks still water-wet in the presence of dense co2 or h2s? Geofluids 12 (4), 280–294.

Ebigbo, A., Golfier, F., Quintard, M., 2013. A coupled, pore-scale model for methanogenic microbial activity in underground hydrogen storage. Adv. Water Resour. 61, 74–85. https://doi.org/10.1016/j.advwatres.2013.09.004.

Ebrahimiyekta, A., 2017. Characterization of geochemical interactions and migration of hydrogen in sandstone sedimentary formations : application to geological storage. Orleans University, France Phd thesis.

Espinoza, Nicolas, Santamarina, Carlos, 2010. Water-CO2-mineral systems: Interfacial tension, contact angle, and diffusion—Implications to CO2 geological storage. Water Resources Research 46 (7). https://doi.org/10.1029/2009WR008634.

Farajzadeh, R., Guo, H., van Winden, J., Bruining, J., 2017. Cation exchange in the presence of oil in porous media. ACS Earth Space Chem. 1 (2), 101–112. https://doi.org/10.1021/acsearthspacechem.6b00015.

Farokhpoor, R., Bjørkvik, B.J., Lindeberg, E., Torsæter, O., 2013. Wettability behaviour of co2 at storage conditions. Int. J. Greenhouse Gas Control 12, 18–25. https://doi.org/10.1016/j.ijggc.2012.11.003.

Flesch, S., Pudlo, D., Albrecht, D., Jacob, A., Enzmann, F., 2018. Hydrogen underground storage-petrographic and petrophysical variations in reservoir sandstones from laboratory experiments under simulated reservoir conditions. Int. J. Hydrogen Energy 43 (45), 20822–20835. https://doi.org/10.1016/j.ijhydene.2018.09.112.

Gabrielli, P., Poluzzi, A., Kramer, G.J., Spiers, C., Mazzotti, M., Gazzani, M., 2020. Seasonal energy storage for zero-emissions multi-energy systems via underground hydrogen storage. Renew. Sustain. Energy Rev. 121, 109629. https://doi.org/10.1016/j.rser.2019.109629.

Haeri, F., Tapriyal, D., Sanguinito, S., Shi, F., Fuchs, S.J., Dalton, L.E., Baltrus, J., Howard, B., Crandall, D., Matranga, C., Goodman, A., 2020. Co2–brine contact angle measurements on navajo, nugget, bentheimer, bandera brown, berea, and mt. simon sandstones. Energy Fuel. 34 (5), 6085–6100. https://doi.org/10.1021/acs.energyfuels.0c00436.

Hagemann, B., Panfilov, M., Ganzer, L., 2016. Multicomponent gas rising through water with dissolution in stratified porous reservoirs - application to underground storage of h2 and co2. J. Nat. Gas Sci. Eng. 31, 198–213. https://doi.org/10.1016/j.jngse.2016.03.019.

Hashemi, L., Blunt, M., Hajibeygi, H., 2021. Pore-scale modelling and sensitivity analyses of hydrogen-brine multiphase flow in geological porous media. Sci. Rep. 11 (1), 8348. https://doi.org/10.1038/s41598-021-87490-7.

Heinemann, N., Alcalde, J., Miocic, J.M., Hangx, S.J.T., Kallmeyer, J., Ostertag-Henning, C., Hassanpouryouzband, A., Thaysen, E.M., Strobel, G.J., Schmidt-Hattenberger, C., Edlmann, K., Wilkinson, M., Bentham, M., Stuart Haszeldine, R., Carbonell, R., Rudloff, A., 2021. Enabling large-scale hydrogen storage in porous media - the scientific challenges. Energy Environ. Sci. 14, 853–864. https://doi.org/10.1039/D0EE03536J.

Iglauer, S., Ali, M., Keshavarz, A., 2021. Hydrogen wettability of sandstone reservoirs: implications for hydrogen geo-storage. Geophys. Res. Lett. 48 (3). https://doi.org/10.1029/2020GL090814. e2020GL090814.

Jung, J.-W., Wan, J., 2012. Supercritical co2 and ionic strength effects on wettability of silica surfaces: equilibrium contact angle measurements. Energy Fuel. 26 (9), 6053–6059. https://doi.org/10.1021/ef300913t.

Kapetas, L., Vincent-Bonnieu, S., Farajzadeh, R., Eftekhari, A., Mohd-Shafian, S., Bahrim, R.K., Rossen, W., 2015. Effect of permeability on foam-model parameters-an integrated approach from coreflood experiments through to foam diversion calculations. In: IOR 2015-18th European Symposium on Improved Oil Recovery. European Association of Geoscientists & Engineers, pp. cp–445.

Kaveh, N.S., Rudolph, E.S.J., van Hemert, P., Rossen, W.R., Wolf, K.H., 2014. Wettability evaluation of a co2/water/bentheimer sandstone system: contact angle, dissolution, and bubble size. Energy Fuel. 28 (6), 4002–4020. https://doi.org/10.1021/ef500034j.

Klise, K.A., Moriarty, D., Yoon, H., Karpyn, Z., 2016. Automated contact angle estimation for three-dimensional x-ray microtomography data. Adv. Water Resour. 95, 152–160. https://doi.org/10.1016/j.advwatres.2015.11.006. Pore scale modeling and experiments.

Kunz, P., Hassanizadeh, S.M., Nieken, U., 2018. A two-phase sph model for dynamic contact angles including fluid–solid interactions at the contact line. Transp. Porous Media 122 (2), 253–277. https://doi.org/10.1007/s11242-018-1002-9.

Laskaris, G., 2015. Effect of surfactant concentration, water treatment chemicals, fatty acids and alcohols on foam behavior in porous media and in bulk.

Li, D., Cheng, P., Neumann, A., 1992. Contact angle measurement by axisymmetric drop shape analysis (adsa). Adv. Colloid Interface Sci. 39, 347–382. https://doi.org/10.1016/0001-8686(92)80065-6.

Liu, Z., McClure, J.E., Armstrong, R.T., 2018. Influence of wettability on phase connectivity and electrical resistivity. Phys. Rev. E 98, 043102. https://doi.org/10.1103/PhysRevE.98.043102.

Luboń, K., Tarkowski, R., 2020. Numerical simulation of hydrogen injection and withdrawal to and from a deep aquifer in nw poland. Int. J. Hydrogen Energy 45 (3), 2068–2083. https://doi.org/10.1016/j.ijhydene.2019.11.055.

Mills, J., Riazi, M., Sohrabi, M., 2011. Wettability of common rock-forming minerals in a co2-brine system at reservoir conditions. In: International Symposium of the Society of Core Analysts. Society of Core Analysts Fredericton, Canada, pp. 19–21.

Morrow, N.R., 1975. The effects of surface roughness on contact: angle with special reference to petroleum recovery. J. Can. Pet. Technol. 14 (04), 13. https://doi.org/10.2118/75-04-04.

Nemati, B., Mapar, M., Davarazar, P., Zandi, S., Davarazar, M., Jahanianfard, D., Mohammadi, M., 2020. A sustainable approach for site selection of underground hydrogen storage facilities using fuzzy-delphi methodology. Settl. Spat. Plann. 6, 5–16. https://doi.org/10.24193/JSSPSI.2020.6.02.

Ozarslan, A., 2012. Large-scale hydrogen energy storage in salt caverns. Int. J. Hydrogen Energy 37 (19), 14265–14277. https://doi.org/10.1016/j.ijhydene.2012.07.111. HYFUSEN.

Panfilov, M., 2016. 4 - underground and pipeline hydrogen storage. In: Gupta, R.B., Basile, A., Veziroğlu, T.N. (Eds.), Compendium of Hydrogen Energy. Woodhead Publishing, pp. 91–115. https://doi.org/10.1016/B978-1-78242-362-1.00004-3.

Panfilov, M., Panfilova, I., Toleukhanov, A., Kaltayev, A., 2012. Bio-reactive two-phase transport and population dynamics in underground storage of hydrogen: Natural self-organisation. In: Conference Proceedings, ECMOR XIII - 13th European Conference on the Mathematics of Oil Recovery, Sep 2012, cp-307-00048. European Association of Geoscientists and Engineers, p. 265. https://doi.org/10.3997/2214-4609.20143214.

Peksa, A.E., Wolf, K.-H.A., Zitha, P.L., 2015. Bentheimer sandstone revisited for experimental purposes. Mar. Pet. Geol. 67, 701–719. https://doi.org/10.1016/j.marpetgeo.2015.06.001.

Prydatko, A.V., Belyaeva, L.A., Jiang, L., Lima, L.M.C., Schneider, G.F., 2018. Contact angle measurement of free-standing square-millimeter single-layer graphene. Nat Commun 9 (1), 4185. https://doi.org/10.1038/s41467-018-06608-0.

Rudolph, T., 2019. Underground hydrogen storage–current developments and opportunities. In: EAGE/DGMK Joint Workshop on Underground Storage of Hydrogen, 2019. European Association of Geoscientists & Engineers, pp. 1–2.

Rücker, M., Bartels, W.-B., Singh, K., Brussee, N., Coorn, A., van der Linde, H.A., Bonnin, A., Ott, H., Hassanizadeh, S.M., Blunt, M.J., Mahani, H., Georgiadis, A., Berg, S., 2019. The effect of mixed wettability on pore-scale flow regimes based on a flooding experiment in ketton limestone. Geophys. Res. Lett. 46 (6), 3225–3234. https://doi.org/10.1029/2018GL081784.

Sainz-Garcia, A., Abarca, E., Rubi, V., Grandia, F., 2017. Assessment of feasible strategies for seasonal underground hydrogen storage in a saline aquifer. Int J Hydrogen Energy 42 (26), 16657–16666. https://doi.org/10.1016/j.ijhydene.2017.05.076.

Stevar, M.S., Böhm, C., Notarki, K.T., Trusler, J.M., 2019. Wettability of calcite under carbon storage conditions. Int. J. Greenhouse Gas Control 84, 180–189. https://doi.org/10.1016/j.ijggc.2019.03.024.

Stone, H.B.J., Veldhuis, I., Richardson, R.N., 2009. Underground hydrogen storage in the uk. Geolog. Soc. Lond. Spec. Publ. 313 (1), 217–226. https://doi.org/10.1144/SP313.13. https://sp.lyellcollection.org/content/313/1/217.full.pdf.

Tarkowski, R., 2019. Underground hydrogen storage: characteristics and prospects. Renew. Sustain. Energy Rev. 105, 86–94. https://doi.org/10.1016/j.rser.2019.01.051.

Wang, S., Edwards, I.M., Clarens, A.F., 2013. Wettability phenomena at the co2–brine–mineral interface: implications for geologic carbon sequestration. Environ. Sci. Technol. 47 (1), 234–241.

Yang, D., Gu, Y., Tontiwachwuthikul, P., 2008. Wettability determination of the reservoir brine- reservoir rock system with dissolution of co2 at high pressures and elevated temperatures. Energy Fuel. 22 (1), 504–509.

Yang, S.-Y., Hirasaki, G., Basu, S., Vaidya, R., 1999. Mechanisms for contact angle hysteresis and advancing contact angles. J. Petrol. Sci. Eng. 24 (2), 63–73. https://doi.org/10.1016/S0920-4105(99)00049-2.

Yekta, A.E., Manceau, J.C., Gaboreau, S., Pichavant, M., Audigane, P., 2018. Determination of hydrogen–water relative permeability and capillary pressure in sandstone: application to underground hydrogen injection in sedimentary formations. Transp. Porous Media 122 (2), 333–356. https://doi.org/10.1007/s11242-018-1004-7.